5th International IEEE Vehicle Power and Propulsion Conference

September 7 – 11, 2009, Dearborn, Michigan, USA

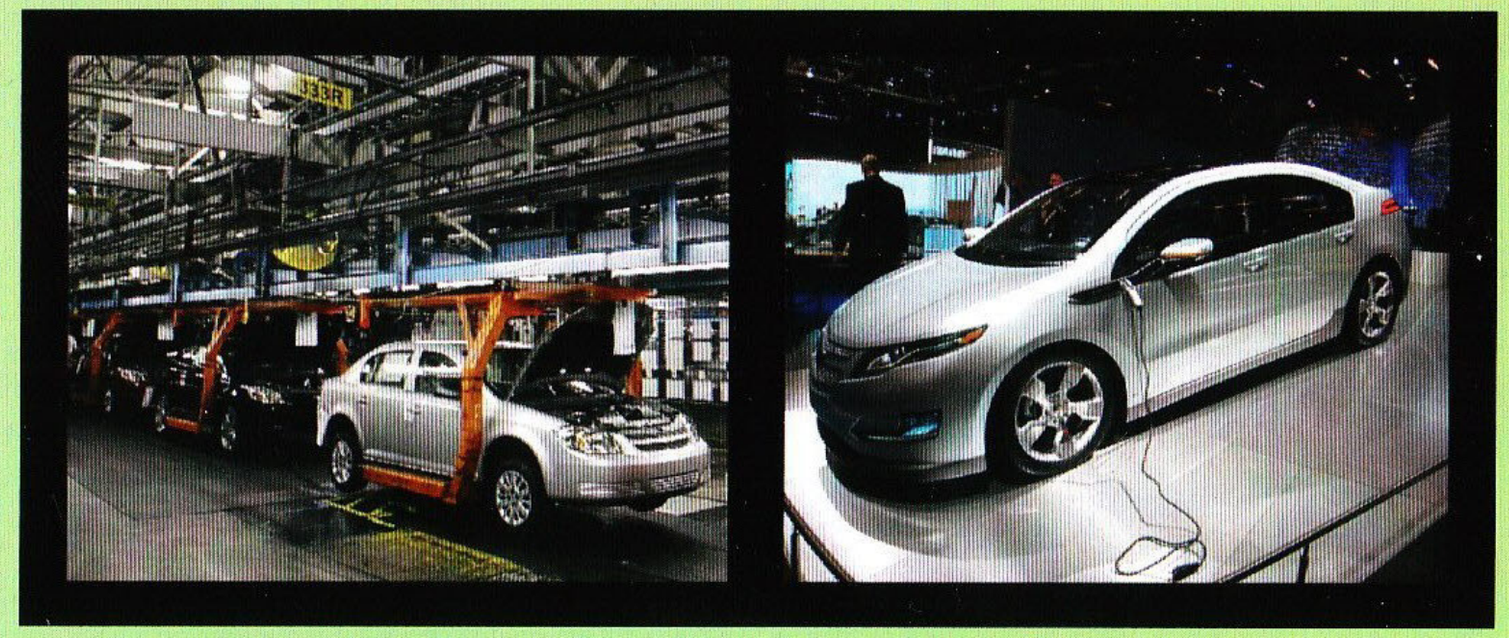

IEEE
Celebrating 125 Years
of Engineering the Future

pels

IEEE VTS
Connecting the Mobile World

IEEE Catalog Number: CFP09VPP-CDR
ISBN: 978-1-4244-2601-0
Library of Congress: 2008904864

PS02-13 **Fault Detection and Location of Open-Circuited Switch Faults in Matrix Converter Drive Systems**
Sangshin Kwak; *Daegu University, Korea.*
Taehyung Kim; *University of Michigan-Dearborn, USA.*

PS02-14 **The Study on the Synthetic Performance Evaluation Method of HEV Motor Propulsion System**
Li Jiong, Wang Jun; *Academy of Armored Force Engineering, China.*

PS02-15 **Flux-Barrier Design Technique for Improving Torque Performance of Interior Permanent Magnet Synchronous Motor for Driving Compressor In HEV**
Liang Fang, Jung-Pyo Hong; *Hanyang University, Korea*

PS02-16 **Characteristics and Radial Magnetic Force of Interior Permanent Magnet Synchronous Motor According to Pole/Slot Combinations**
Soon-O Kwon, Jeong-Jong Lee, Tao Sun, Jung-Pyo Hong; *Hanyang University, Korea.*

PS03-1 **A Novel Control Scheme of Propulsion Motor for Integrated Powertrain of Electric Bus**
Hong Fu, Guangyu Tian, Quanshi Chen; *Tsinghua University, China.*
Yaobin Chen, *Indianapolis University-Purdue University Indianapolis, USA.*

PS03-2 **Motor Motion Control of Automobile Steer-By-Wire System in Electric Vehicles**
Yu Lei-Yan, Yun Ping-Li; *China University of Petroleum, China.*

PS03-3 **Controlling Lunar Lander in Powered Descending Phase**
Xiaofei Chang, Weiwei Yu, Jie Yan; *Northwestern Polytechnical University, China.*

Flux-Barrier Design Technique For Improving Torque Performance of Interior Permanent Magnet Synchronous Motor For Driving Compressor In HEV

Liang Fang, Jung-Pyo Hong, *Senior Member, IEEE*
Department of Automotive Engineering
Hanyang University
Seoul 133-791, Korea
fangliang@hanyang.ac.kr, hongjp@hanyang.ac.kr

***Abstract*—This paper presents flexible flux-barrier designs in an interior permanent magnet synchronous motor (IPMSM) for driving compressor in hybrid electrical vehicle. A conventional single-layer IPMSM model, a popular double-layer IPMSM model and a proposed novel double-barrier IPMSM model are built and optimized for improving torque performance by reducing cogging torque and torque ripple. The novel double-barrier IPMSM has beneficial attributes of simplest single-layer PM and flexible double pairs of flux-barriers in IPM rotor design. The optimal geometries of flux-barriers in each IPMSM designs are determined by response surface methodology (RSM). The cogging torque and torque ripple of IPMSM model are calculated using finite element analysis (FEA), and confirmed by test. Finally, the effectivity of the novel double-barrier IPMSM design on torque performance improvement is well proved, and its advantages are emphasized.**

Keywords-FEA; IPMSM; RSM; single-layer/double-layer/novel double-barrier IPMSM deisgn; cogging torque and torque ripple

I. INTRODUCTION

The interior permanent magnet synchronous motors (IPMSM) are widely used in automotive and other servo derive due to their superior advantages, such as high efficiency, high torque density and wide speed range operation [1]. However, the significant torque pulsation is an inherent drawback of IPMSM, which results in mechanical resonance, vibration, acoustic noise and damage to drive components [2], [3]. Therefore, the reduction of torque pulsation for motor smooth running is always required as the improvement of torque performance. Many papers talked this problem, and proposed some effective approaches for reducing torque pulsation. In this paper, torque ripple and cogging torque, as the main components of torque pulsation are focused to be removed, while the lower total harmonic distortion (THD) of back electromotive force is desired in toque performance improving.

The conventional single-layer design IPMSM has only one pair of flux-barriers with each single PM piece in rotor iron, which benefits easy manufacture. And the popular double-layer design IPMSM is attractive since their flexible double pairs of flux-barriers can be used to distribute PM flux in rotor. In addition, this paper proposes a novel IPMSM design features double flux-barriers created with single-layer PM piece.

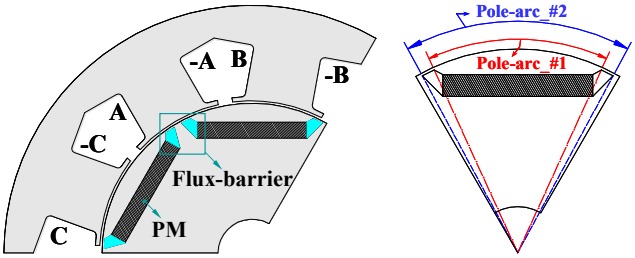

Figure 1. Configuration of conventional single-layer IPMSM model.

By performing the response surface methodology (RSM), the geometries of buried flux-barriers in mentioned IPMSM models are optimized. Finite element analysis (FEA) is used to analyze torque characteristics, and their validity are confirmed by tests. The effectivity of presented various flux-barrier designs in IPMSM on torque pulsation reduction is examined.

II. MODEL AND CHARACTERISTIC ANALYSIS

A. Prototype Analysis Model

Fig. 1 shows a prototype 6-pole/9-slot IPMSM model for a driving compressor in a hybrid electric vehicle (HEV). The main dimension and specifications are listed in TABLE I. The stator has 3-phase concentrated windings, and the rotor adopts conventional single-layer IPM design. The magnet pole-arc is determined by its flux-barrier design in term of pole-arc_#1 and pole-arc_#2, with considering the width of rib region.

TABLE I
DIMENSION AND SPECIFICATIONS OF DRIVING COMPRESSOR IPMSM

Items	Value	Unit
Stator outer diameter	117.2	mm
Rotor outer diameter	70.8	mm
Stack length	15	mm
Air-gap length	0.6	mm
B_r (@20~25°C)	1.22~1.28	T
Maximum terminal voltage	98.6	V
Rated output power	2	kW
Maximum current	17	A_{rms}
Base speed	3500	rpm

978-1-4244-2601-0/09/$25.00 ©2009 IEEE

B. Torque Characteristic Analysis

In this paper, the output torque characteristic of IPMSM are predicted by using equivalent circuit method, which based on the precious machine parameters calculated by FEA, such as *d-*, *q*-axis inductances and back electromotive force (Back-EMF).

In a *d-q* reference frame, a proved equivalent circuit with iron loss consideration is given, as Fig. 2 illustrates [4], [5]. And the corresponding mathematical models of *d-q* axis circuit are obtained as: voltages and currents are given as equations (1) and (2), and output torque is expressed as equations (3).

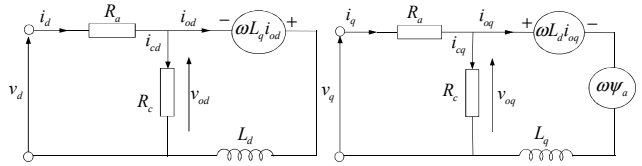

(a) *d*-axis equivalent circuit (b) *q*-axis equivalent circuit

Figure 2. Equivalent circuits of IPMSM

$$\begin{bmatrix} v_d \\ v_q \end{bmatrix} = R_a \begin{bmatrix} i_{od} \\ i_{oq} \end{bmatrix} + \left(1 + \frac{R_a}{R_c}\right) \begin{bmatrix} v_{od} \\ v_{oq} \end{bmatrix} + p \begin{bmatrix} L_d & 0 \\ 0 & L_q \end{bmatrix} \begin{bmatrix} i_{od} \\ i_{oq} \end{bmatrix} \tag{1}$$

$$\begin{bmatrix} v_{od} \\ v_{oq} \end{bmatrix} = \begin{bmatrix} 0 & -\omega L_d \\ \omega L_d & 0 \end{bmatrix} \begin{bmatrix} i_{od} \\ i_{oq} \end{bmatrix} + \begin{bmatrix} 0 \\ \omega \psi_a \end{bmatrix} \tag{2}$$

$$\begin{aligned} T &= P_n[\psi_a i_q + (L_d - L_q) i_d i_q] \\ &= P_n[\psi_a I_a \cos\beta + \frac{1}{2}(L_d - L_q) I_a^2 \sin 2\beta] \end{aligned} \tag{3}$$

where i_d, i_q: *d-*, *q*-axis components of armature current; v_d, v_q: *d-*, *q*-axis components of terminal voltage; ψ_a: $\sqrt{3/2}\,\psi_f$; ψ_f: maximum flux linkage of permanent magnet; R_a: armature winding resistance; R_c: iron loss equivalent resistance, L_d, L_q: inductance along *d-*, *q*-axis; $p = d/dt$; P_n: number of pole pairs.

From the torque equation (3), the output torque is predicted according to the input armature current I_a and its phase angle β [4]. Therefore, L_d and L_q must be computed according to the variations of I_a and β, and ψ_a is obtained from the fundamental component of Back-EMF characteristic. In this paper, L_d and L_q are estimated by FEA with equation (4). The steady-state phasor diagram of IPMSM is displayed in Fig. 3 [5].

$$L_d = \frac{\psi_o \cos\alpha - \psi_a}{i_d} \qquad L_q = \frac{\psi_o \sin\alpha}{i_q} \tag{4}$$

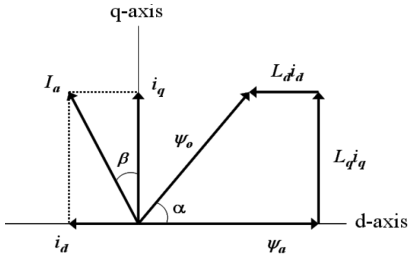

Figure 3. Phasor diagram of IPMSM.

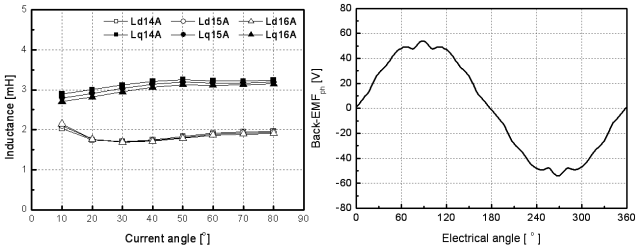

(a) *d-*, *q*- axis inductances (b) Back-EMF@3500rpm

Figure 4. Inductance and Back-EMF of IPMSM model calculated by FEA

where ψ_o: total flux linkage considering the armature reaction effects; α: phase difference between ψ_a and ψ_o.

By performing the above *d-q* axis equivalent circuits, the output performances of IPMSM can be predicted quickly. In the simulation, the following limitations of armature current and terminal voltage are considered:

$$V_a = \sqrt{{v_d}^2 + {v_q}^2} \le V_{am}$$

$$I_a = \sqrt{{i_d}^2 + {i_q}^2} \le I_{am}$$

where, I_{am}, V_{am}: constrain values of current and voltage.

The entire speed range operation considering the above control conditions is acquired in the following manner. In the anterior region of base speed, maximum torque per ampere control is employed, and flux weakening control is applied in the posterior region. Fig. 5 shows the results of speed versus torque and output performance, also the input current and its phase angle. Therefore, the torque characteristic at any speed operation can be calculated by FEA. In this study, the rated torque operated at base speed 3500[rpm] is focused, and its torque ripple and cogging torque are desired to be reduced.

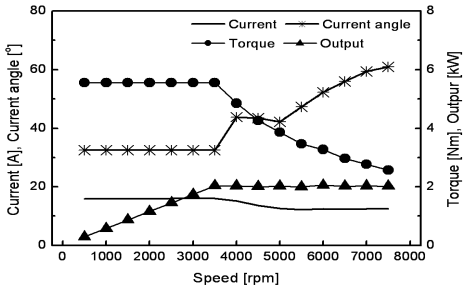

Figure 5. Speed versus torque and output performance of IPMSM model.

C. Flexible Flux-barrier Design

The effectivity of various flux-barrier designs in IPMSM on torque pulsation reduction is examined in this study. Base on the prototype single-layer IPMSM model, a double-layer IPMSM model is built by splitting the same amount of PM into thin pieces. This accordingly creates two pairs of separated flux-barriers which can be used to flexibly distribute the rotor part PM flux crossing into air-gap form desired magnetic field, as Fig. 6(a) illustrates. On the other hand, it should be noticed that the double-layer IPM design will unavoidably increase the manufacture cost and difficulty, and even may cause severe irreversible demagnetization in the created thin PM pieces.

In this paper, a novel double-barrier IPM rotor model is proposed, as Fig. 6(b) illustrates. The buried single-layer PM has two pairs of connected flux-barriers, by which the PM flux in rotor part is also dispersed effectively. For crossing magnetic flux distribution, it is similar to the feature of double-layer IPM design, but decreased the cost and difficult in manufacture.

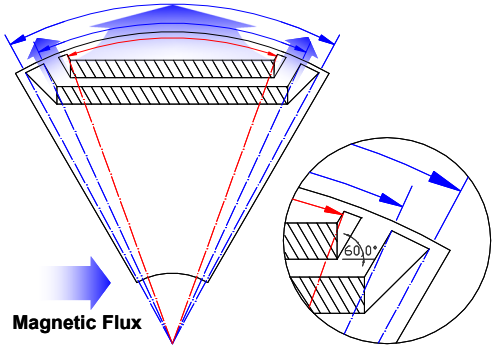

(a) Double-layer IPM rotor design

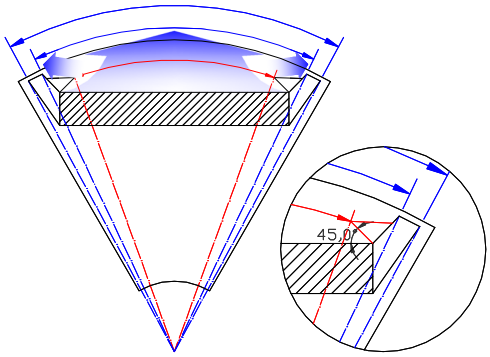

(b) Double-barrier IPM rotor design

Figure 6. Double pairs of flux-barrier designs based on prototype IPM rotor

III. Optimization of Flux-barriers in IPMSM

The IPM rotor inner geometry design is very complicated owing to many design factors, and also mechanical robustness between each part must be fully considered in modeling [4]. In this paper, the presented flux-barrier designs in IPM rotor are optimized by introducing response surface methodology (RSM). As an effective approach, RSM is usually applied for searching the optimal design of electrical devices in order to improve machine performances [6]. It is a set of statistical and mathematical techniques to find the "best fitted" response of the physical system through experiment or simulation [7].

TABLE II
RANGES OF DESIGN VARIABLES FOR OPTIMIZATION IN RSM

Analysis IPMSM Model	**Pole-arc #0** [Outer layer]	**Pole-arc #1** [Inner layer]	**Pole-arc #2** [Inner layer]
Single-layer design		41°~48°	54.2°~59.2°
Double-layer design	35.4°~41°	46°~52°	54.2°~59.2°
Double-barrier design	35.4°~41°	46°~52°	54.2°~59.2°

* Outer layer: the upper PM layer closing to rotor surface.
* Pole-arc #0 is defined for describing the inner pole-arc of "Outer-layer".

For examining the influence of flux-barriers design on torque pulsation reduction, only the magnet pole-arcs, which defined by flux-barriers variation as shown in Fig. 1, are chosen as design variables in RSM analysis. For decreasing design difficulty, three variables are chosen to describe the two pairs of flux-barriers in IPM rotor designs, with the non-significant variable fixed to be proper constant, as Fig. 6 gives.

Here, the optimal design of double-layer IPMSM model by RSM is taken for example. Table II lists the experiment range of each design variables [Pole-arc_#0, Pole-arc_#1 and Pole-arc_#2] in RSM analysis, and the simulation models are built according to the full factorial combinations of design variables. With the above three design variables, fifteen different models are required to be analyzed in RSM, as TABLE III lists.

In the RSM optimization analysis, the design objectives are determined as: toque ripple at rated operation low than 10[%] and cogging torque amplitude (peak-peak value) less than 3[%] of rated torque 5.5[Nm], nearly 0.165[Nm], in addition THD of Back-EMF low than 4.0[%] is required. On the other hand, the output torque and power constraints are given as followings:

- Design objectives:

$$\mathbf{Y}_{\text{Trip}} \le 10.0[\%], \quad \mathbf{Y}_{\text{CT(p-p)}} \le 0.16[\text{Nm}], \quad \mathbf{Y}_{\text{THD}} \le 4.0[\%]$$

- Subject to:

$$\mathbf{Y}_{\text{Tave}} \ge 5.5[\text{Nm}], \quad \text{Output power} \ge 2[\text{kW}]$$

The responses of design objectives with all design variables are displayed in Fig. 7. It is found the desired minimum points of torque ripple and cogging torque can not be achieved at the same design point. Therefore, the optimum point is selected as possible as close to the design objectives, as "broken crossing lines" shows. Finally, under satisfying all design objectives, the optimal double-layer design IPMSM model is built using the corresponding design variables as TABLE IV lists.

TABLE III
DESIGN VARIABLES AND RESPONSES OF RSM SIMULATION

P-arc_#0	**P-arc_#1**	**P-arc_#2**	$\mathbf{Y}_{\text{Trip}}$	$\mathbf{Y}_{\text{CT(P-P)}}$	$\mathbf{Y}_{\text{THD}}$
36.5°	47.35°	55.15°	15.86	0.055	3.05
39.8°	47.35°	55.15°	15.23	0.156	4.04
36.5°	50.8°	55.15°	12.57	0.088	3.32
39.8°	50.8°	55.15°	12.50	0.090	3.96
36.5°	47.35°	58.15°	14.60	0.055	3.61
39.8°	47.35°	58.15°	13.51	0.150	4.57
36.5°	50.8°	58.15°	10.54	0.087	4.84
39.8°	50.8°	58.15°	9.56	0.084	5.39
35.4°	49.08°	56.65°	10.75	0.176	4.08
41.0°	49.08°	56.65°	11.07	0.140	4.41
38.15°	46.0°	56.65°	14.41	0.087	5.01
38.15°	52.0°	56.65°	10.41	0.054	4.38
38.15°	49.08°	54.2°	15.83	0.092	3.55
38.15°	49.08°	59.2°	14.23	0.087	5.00
38.15°	49.08°	56.65°	12.89	0.091	4.22

* " " : according to the variables experiment ranges as TABLE I lists.
* Units of design objectives: $\mathbf{Y}_{\text{Trip}}$ [%], $\mathbf{Y}_{\text{CT(p-p)}}$ [Nm], $\mathbf{Y}_{\text{THD}}$ [%],

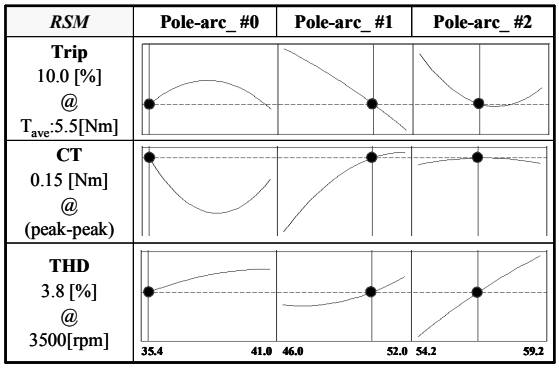

Figure 7. Responses of design objectives based on design variables in RSM

TABLE IV
OPTIMAL VARIABLES OF FLUX-BARRIERS DESIGNS IN IPMSMS

Optimal Model	Pole-arc #0	Pole-arc #1	Pole-arc #2
Single-layer design		46.0°	58.0°
Double-layer design	35.4°	50.4°	56.6°
Double-barrier design	36.0°	52.0°	59.0°

IV. RESULT AND DISCUSS

Torque performance is improved by reducing torque ripple and cogging torque through optimizing the buried flux-barriers in each IPMSM models as presented. The "optimal" results predicted in RSM should be confirmed by FEA. The optimized IPMSM models are built with corresponding "fittest value" of design variables determined by RSM, as TABLE IV lists.

The optimized double-layer design IPMSM model is fabricated and tested for confirming the validity of calculated results by FEA. Furthermore, the calculated torque ripple, cogging torque and Back-EMF characteristics of the optimized three IPMSM models using proved method are compared for examining the effectivity of these various flux-barrier designs on torque pulsation reduction.

A. Test of Double-layer IPMSM

The fabricated double-layer IPMSM is tested, as Fig. 8 shows. The torque ripple at rated operation is tested by inputting current 15.3[Arms] with phase angle β=32.5°. It is found that the tested result 7.8[%] is lower than the FEA result 10.0[%], as Fig. 9 shows. The error is thought caused by the influence of the reduction gear inertial. The cogging torque and Back-EMF characteristics are tested and the measured results shows good agreement with FEA results, as Fig. 10 and Fig. 11 show. The slightly different may be caused by manufacturing.

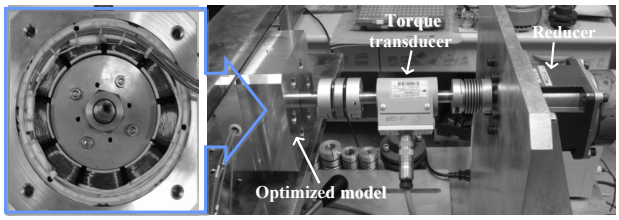

Figure 8. Output torque test of fabricated optimized double-layer IPMSM

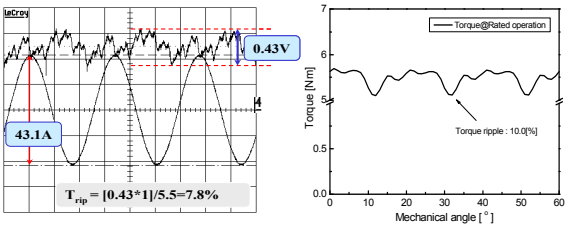

(a) Test result [1V indicates 1Nm] (b) FEA result

Figure 9. Output torque performance comparison @Rated torque=5.5[Nm]

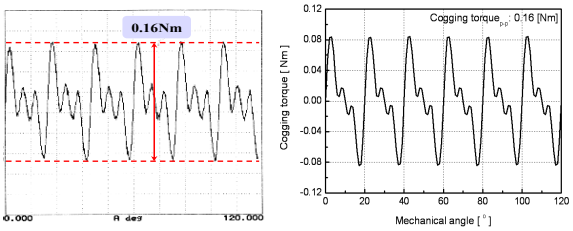

(a) Test result (b) FEA result

Figure 10. Cogging torque characteristic comparison

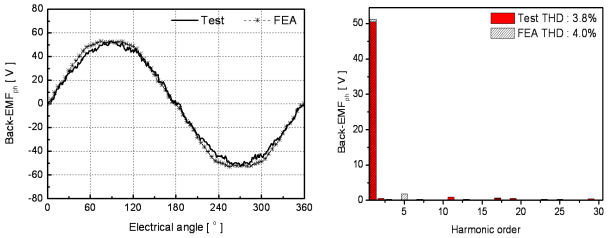

Figure 11. Back-EMF and THD characteristics comparison @3500rpm

B. Torque Ripple and Cogging Torque Comparison

Fig. 12 illustrates the geometries of the three optimized flux-barriers designs in IPMSM rotor models. The mechanical robustness is considered by margining 0.5[mm] rib between the flux-barrier and rotor surface. From their FEA results of output torque and cogging torque, it is found that the double-layer IPM design and proposed novel double-barrier IPM design are both effective for reducing the torque ripple and cogging torque. Compare with the single-layer IPM design, the torque ripple of rated torque reduced from 16.5[%] to 10.0[%] and 7.0[%] separately, and cogging torque relatively decreased 46.7[%] and 66.7[%] of 0.3[Nm] in single-layer IPM design, as Fig. 13 and Fig. 14 show. In other words, the amplitudes of cogging torque are less than 3.0[%] and 1.8[%] of rated torque.

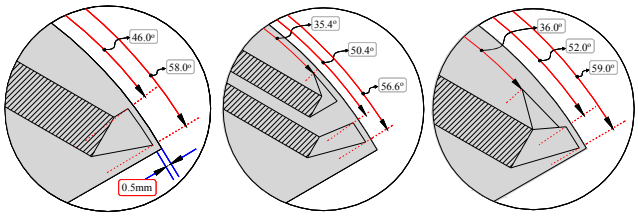

(a) Single-layer design (b) Double-layer design (c) Double-barrier design

Figure 12. Optimized flux-barrier designs in IPMSM rotor model

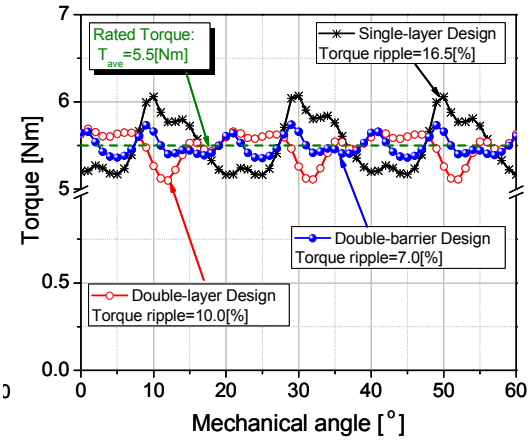

Figure 13. Torque ripple results comparison @FEA

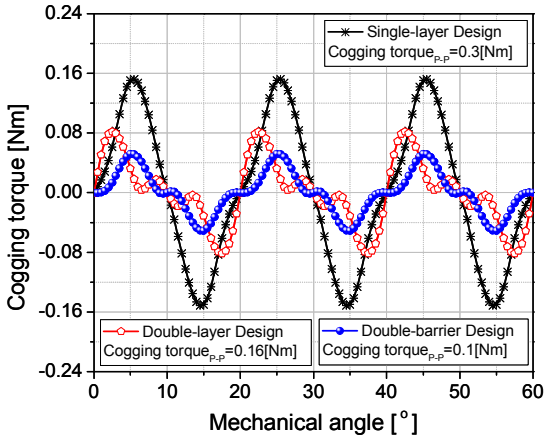

Figure 14. Cogging torque results comparison @FEA

V. CONCLUSION

Torque ripple and cogging torque reduction in IPMSM by optimizing various flux-barrier designs are presented in this paper. In particular, the proposed novel double-barrier IPMSM model, featuring as each single-layer PM piece created double pairs of flux-barriers, has beneficial attribute of the flexible flux-barriers design of double-layer IPMSM, and the simplicity of single-layer IPMSM. The test confirmed output torque and cogging torque comparisons fully proved that the novel double-barrier IPMSM design is more effective design approach for improving torque performance even comparing with the popular double-layer IPMSM design. In conclusion, the proposed novel double-barrier model has simplicity and low-cost advantages for improving IPMSM torque performance.

REFERENCES

[1] John M. Miller, "Propulsion systems for hybrid vehicles", The Institution of Electrical Engineers, 2004.

[2] Nicole Bianchi, Thomas M. Jahns, "Design, Analysis, and Control of Interior PM synchronous Machines", IEEE-IAS Electrical Machines Committee.

[3] Breton, C.; Bartolome, J.; Benito, J.A.; Tassinario, G.; Flotats, I.; Lu, C.W.; Chalmers, B.J, "Influence of machine symmetry on reduction of cogging torque in permanent-magnet brushless motors", *IEEE Trans. Magn.*, *vol. 36, no. 5, Sept. 2000.*

[4] Liang Fang; Jae-woo Jung; Jung-Pyo Hong; Jung-Ho Lee, "Study on High-Efficiency Performance in Interior Permanent-Magnet Synchronous Motor With Double-Layer PM Design," *IEEE Trans. Magn.*, *vol. 44, Issue 11, Part 2, Nov. 2008.*

[5] Ji-Yong Lee, Sang-Ho Lee, Geun-Ho Lee, Jung-Pyo Hong, Jin Hur, "Determination of Parameters Considering Magnetic Nonlinearity in an Interior Permanent Magnet Synchronous Motor," *IEEE Transaction on Magnetics, vol. 402, no. 4, April 2006.*

[6] Sung-Il Kim; Ji-Young Lee; Young-Kyoun Kim; Jung-Pyo Hong; Hur, Y.; Yeon-Hwan Jung, "Optimization for reduction of torque ripple in interior permanent magnet motor by using the Taguchi method," *IEEE Trans. Magn., vol. 41, Issue 5, May 2005.*

[7] L. Qinghua, M. A. Jabbar, and M. Khambadkone, "Response surface methodology based design optimization of interior permanent magnet synchronous motors for wide-speed operation," in *Proc. PEMD*, *vol. 2,* pp. *546-551, March/April 2004.*